Multi-Resolution Reconstructions from Compressive Spectral Coded Projections

Claudia V. Correa
Dept. of Electrical and Computer Engineering
University of Delaware
Newark, DE 19716

Henry Arguello
Dept. of Computer Science
Universidad Industrial de Santander
Bucaramanga, Colombia 680002

Gonzalo R. Arce
Dept. of Electrical and Computer Engineering
University of Delaware
Newark, DE 19716

***Abstract*—Compressive spectral coded projections are attained by an imaging detector as a spatial-spectral field traverses diverse optical elements such as a coded aperture and a dispersive element. Compressed sensing reconstruction algorithms are used to recover the underlying data cube at the resolution enabled by the captured projections. Such reconstructions, however, are computationally expensive because of the data dimensions. In this paper, a multi-resolution (MR) reconstruction approach is presented, such that several versions of the data cube can be recovered at different spatial resolutions, by employing gradient intensity maps. Simulations show that this approach overcomes interpolation results in up to 3dB of PSNR in noisy scenarios.**

***Index Terms*—Compressive spectral imaging, Multi-resolution, Spectral Imaging, Compressed sensing**

I. Introduction

Compressive spectral imaging (CSI) enables the acquisition of spatial information across multiple wavelengths without scanning the region of interest or employing large detectors as required by traditional spectral imaging methods [1]. CSI optical systems are designed such that the 3D (spatial and spectral) information is acquired in lower-dimensional sets of coded projections, i.e. 2-dimensional or single pixel measurements. These occur as the result of the optical phenomena affecting the input source as it passes through different optical devices before being integrated by an imaging detector. The information acquired at the detector is known as compressive coded projections. Several optical architectures implementing CSI principles can be found in the state of the art, including: the coded aperture snapshot spectral imaging system (CASSI) [2], the dual-coded hyper-spectral imager (DCSI) [3], the spatial-spectral encoded compressive hyperspectral imaging system (SSCSI) [4], and the snapshot colored compressive spectral imager (SCCSI) [5]. In general, the sensing process of these architectures can be modeled as the linear system given by $\mathbf{y} = \mathbf{H}\mathbf{f}$, where $\mathbf{y}$ is the set of coded projections; $\mathbf{f}$ is a vector form of the spatial-spectral data cube $\mathbf{F} \in \mathbb{R}^{N\times N\times L}$ with $N \times N$ pixels of spatial resolution and L spectral bands; and $\mathbf{H}$ is the sensing matrix whose structure and entries depend on the optical phenomena induced by the employed devices [6]. Because the number of acquired projections in $\mathbf{y}$ is considerably less than the amount of image voxels to recover, the underlying spatial-spectral data cube is later recovered using numerical optimization methods that seek for a sparse approximation of the data cube $\boldsymbol{\theta} = \boldsymbol{\Psi}^T\mathbf{f}$ in a given basis $\boldsymbol{\Psi}$ [7], [8], by minimizing a cost function of the type

$$\arg\min_{\boldsymbol{\theta}} ||\mathbf{y} - \mathbf{H}\boldsymbol{\Psi}\boldsymbol{\theta}||^2_{\ell_2} + \tau||\boldsymbol{\theta}||_{\ell_1}, \tag{1}$$

with τ as a regularization parameter. Moreover, different cost functions such as low-rank approximations [9], [10] or denoisers in approximate message passing (AMP) [11], [12] can be also used to recover the underlying data. In spite of the fast acquisition process enabled by CSI systems, reconstructions are in general computationally expensive, due to the high dimensions of the involved data. In addition, traditional CSI reconstruction approaches aim at recovering the underlying data cube from the set of coded projections, where the resolution of the reconstruction is as high as the measurements allow. To date, different strategies have been proposed to alleviate the computational cost of CSI reconstructions. These approaches include GPU implementations of reconstruction algorithms [13], separable sensing operators [14]–[16] and block-based reconstructions [17]. Furthermore, general multi-resolution (MR) compressive sensing (CS) frameworks have been recently proposed to recover lower resolution versions instead of the full-resolution signal. For instance, the sum-to-one (STOne) transform proposed in [18] enables fast reconstructions of image previews by appropriately designing the sensing matrix. Given that in CSI the structure of the sensing matrix is determined by the optical configuration of the systems, STOne concepts cannot be directly employed. Another approach presented in [19] establishes that low-resolution (LR) CS reconstructions of an object can be obtained by defining a pair of down-scaling/up-scaling matrices. However, a method to recover a higher-resolution approximation from such LR image is not developed.

This paper presents a multi-resolution (MR) reconstruction approach for CSI that allows to obtain multiple versions of the data cube at different spatial resolutions up to the maximum allowed by the compressed projections, without applying additional super-resolution methods. Specifically, the proposed approach obtains an initial LR reconstruction of the scene at a small scale to estimate the high frequency components of the next scale reconstruction, such that it can be recovered by employing super-pixels on the low-frequency areas of the scene. A gradient intensity image is used to

ISBN 978-90-827970-1-5

develop a decimation matrix that modifies the original sensing matrix $\mathbf{H}$, to generate the equivalent MR sensing matrix that is later used in a CS reconstruction algorithm. The process can be sequentially performed up to the maximum resolution allowed by the captured projections. Simulations on two different data cubes with the CASSI architecture are used to test the performance of the proposed approach.

II. Compressive Spectral Imaging Problem in CASSI

The coded aperture snapshot spectral imaging system (CASSI) [1], [2] is one of the most remarkable CSI architectures, for this reason it is used in this paper to describe and test the proposed MR reconstruction approach that will be presented in Section III. CASSI projections are obtained as the result of applying two main operations: spatial coding realized by a coded aperture $T(x,y)$ and dispersion, as illustrated in Fig. 1. Specifically, the input source $f_0(x,y,\lambda)$ is first modulated by $T(x,y)$, where (x,y) represent the spatial dimensions and λ the spectral components. This modulation consists on either blocking the light at each spatial location or letting it to pass through. After that, the encoded source is spectrally decomposed by the dispersive element, and the 2D compressed projections are obtained as the integration of the coded and dispersed source over the spectral dimension at the focal plane array (FPA).

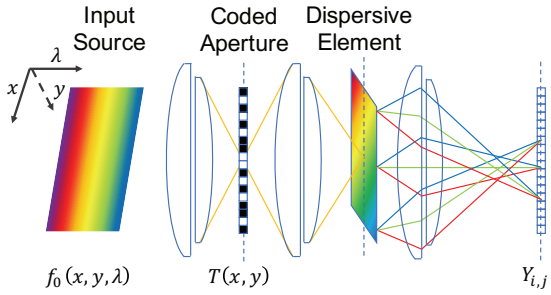

Fig. 1. Top view schematic representation of the CASSI optical architecture.

Assuming a discrete representation of the input data cube $\mathbf{F}$ composed by L spectral bands, each with $N \times N$ pixels of spatial resolution, and the pixelated $N \times N$ coded aperture $\mathbf{T}$, the intensity value captured at the (i,j)-th pixel of the detector can be written as

$$Y_{i,j} = \sum_{k=1}^{L} F_{i,j-k,k} T_{i,j-k} + \omega_{i,j}, \tag{2}$$

where ω is the noise of the system. When several snapshots $\left\{\mathbf{Y}^{\ell}\right\}_{\ell=0}^{K-1}$ are captured, their vector forms can be stacked in a single column $\mathbf{y} = \left[\left(\mathbf{y}^{0}\right)^{T}, \cdots, \left(\mathbf{y}^{K-1}\right)^{T}\right]$. Thus, as in the general case of CSI systems, the CASSI forward model for acquiring a $N \times N \times L$ data cube is given by the linear system

$$\mathbf{y} = \mathbf{H}\mathbf{f}, \tag{3}$$

where $\mathbf{f} \in \mathbb{R}^{v}$ is a vector form of the data cube with $v = N^2 L$, and $\mathbf{H}$ is the sensing matrix accounting for all K snapshots [20].

III. Multi-Resolution Reconstruction Approach

Instead of attaining CSI reconstructions at the highest spatial resolution allowed by the acquired projections, by solving the problem in (1), this paper proposes to recover multiple versions of the same data cube at different spatial resolutions. This approach first assumes that a low resolution version of the data cube can be obtained as

$$\mathbf{f}_{\Delta} = \mathbf{D}_{\Delta}\mathbf{f}, \tag{4}$$

where $\mathbf{D}_{\Delta} \in \mathbb{R}^{\frac{v}{4^{\Delta}} \times v}$ is a decimation matrix that yields a $\frac{N}{2^{\Delta}} \times \frac{N}{2^{\Delta}} \times L$ object, with Δ representing an integer parameter for the decimation factor. Note that in this work, the decimation is applied only to the spatial dimensions and, for simplicity the decimation factor is expressed as a power of 2, which means that the spatial dimensions of $\mathbf{f}_{\Delta}$ are $1/2^{\Delta}$ the dimensions of $\mathbf{f}$. Similarly, the high-resolution spectral image can be obtained as $\mathbf{f} = \mathbf{D}_{\Delta}^{-1}\mathbf{f}_{\Delta}$, where $\mathbf{D}_{\Delta}^{-1}$ represents an up-scaling operator, which is not necessarily the inverse of $\mathbf{D}_{\Delta}$. Therefore, using (4) in (3) we can obtain the equivalent sensing model for the low-resolution data cube as

$$\mathbf{y} = \tilde{\mathbf{H}}\mathbf{f}_{\Delta} + \epsilon, \tag{5}$$

where $\tilde{\mathbf{H}} = \mathbf{H}\mathbf{D}_{\Delta}^{-1}$ is the equivalent sensing matrix for the low resolution scene and, $\epsilon = \mathbf{H}\left(\mathbf{I} - \mathbf{D}_{\Delta}^{-1}\mathbf{D}_{\Delta}\right)\mathbf{f}$ is an approximation error due to the down/up-scaling operations [19]. Then, an estimation of $\boldsymbol{\theta}_{\Delta}$, a sparse representation of $\mathbf{f}_{\Delta}$, can be obtained by solving the low resolution problem given by

$$\arg\min_{\boldsymbol{\theta}_{\Delta}} ||\mathbf{y} - \tilde{\mathbf{H}}\boldsymbol{\Psi}_{\Delta}\boldsymbol{\theta}_{\Delta}||_{\ell_2}^2 + \tau||\boldsymbol{\theta}_{\Delta}||_{\ell_1}, \tag{6}$$

where $\boldsymbol{\Psi}_{\Delta}$ is the sparse representation basis for that particular resolution. Note that (6) presents a shrinked version of the minimization problem from (1). The low resolution scene can be subsequently obtained as the inverse sparse transformation $\hat{\mathbf{f}}_{\Delta} = \boldsymbol{\Psi}_{\Delta}^{-1}\boldsymbol{\theta}_{\Delta}$. To illustrate the error induced by the low resolution approximation in (5), Fig. 2 presents an example of normalized ϵ for a test data cube using three different decimation factors, i.e. $\Delta = 1, 2, 3$, which correspond to a half, one quarter and one eight the original resolution. It is evident that most of the errors are concentrated around high frequency pixels, which motivates the exploitation of gradient intensity maps in the up-scaling process.

One way to obtain an up-scaled version of $\mathbf{f}_{\Delta}$ is to apply an interpolation algorithm, however, for large decimation factors, these methods fail on approximating the high frequency regions of the scene. Thus, the proposed approach exploits the gradient intensity images of the low resolution reconstruction to generate a multi-resolution (MR) decimation matrix $\mathbf{D}_{\Delta}$ such that an up-scaled version of the data cube can be recovered by solving the problem in (6) using the corresponding MR matrix. Specifically, the MR decimation matrix is built using

ISBN 978-90-827970-1-5

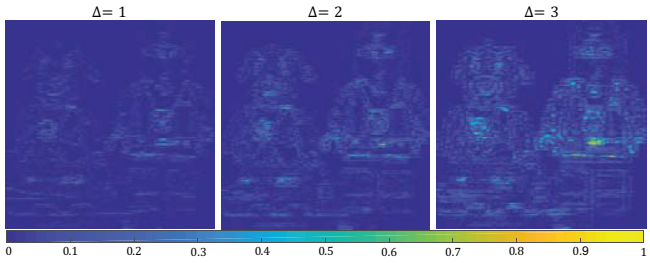

Fig. 2. Low-resolution normalized approximation errors ϵ from (5) for different decimation factors Δ. The errors are concentrated around the high frequency regions of the scene.

two different decimation factors, i.e. 2^{Δ} for smooth regions and $2^{\Delta-1}$ for pixels indexed as edges by the map of intensity gradient. The algorithm can iterate on this process using the intensity gradient of the resulting reconstruction to calculate a new MR decimation matrix, until the maximum resolution is reached. In the following, the main steps of the proposed MR reconstruction approach are described. Let $\hat{\mathbf{f}}_{\Delta}$ be the initial low resolution reconstruction which can be rearranged as the data cube $\hat{\mathbf{F}}_{\Delta} = \left[\hat{\mathbf{F}}^{1}_{\Delta}, \cdots, \hat{\mathbf{F}}^{L}_{\Delta}\right]$, where $\hat{\mathbf{F}}^{\ell}_{\Delta}$ refers to the ℓ-th spectral band. Then, the intensity gradient map of each spectral band can be calculated using any edge detection method such as Canny or Sobel filters. The intensity gradient for the ℓ-th spectral band is given by the derivatives along the x and y axes and can be written as

$$\frac{\partial \hat{\mathbf{F}}^{\ell}_{\Delta}}{\partial x \partial y} = \mathbf{P} * \hat{\mathbf{F}}^{\ell}_{\Delta}, \tag{7}$$

where $\mathbf{P}$ represents the gradient operator and $*$ a convolution. Since spectral images typically exhibit high spatial correlation across bands, the intensity gradient map for the whole data cube can be expressed as the sum of the L intensity gradients

$$\mathbf{E}_{\Delta} = \sum_{\ell=1}^{L} \mathbf{P} * \hat{\mathbf{F}}^{\ell}_{\Delta}. \tag{8}$$

The resulting intensity gradient map $\mathbf{E}_{\Delta}$ is then used to estimate the high frequency elements of the up-scaled data cube with spatial resolution $\frac{N}{2^{\Delta-1}} \times \frac{N}{2^{\Delta-1}}$. Because the spatial resolution of the data cube to be recovered doubles the current resolution, its intensity gradient map can be estimated as $\mathbf{E}_{\Delta-1} = \mathbf{E}_{\Delta} \otimes \mathbf{1}_2$, where $\mathbf{1}_2$ is a 2×2 all-ones matrix, and $\otimes$ is the matrix Kronecker product. Elements in $\mathbf{E}_{\Delta-1}$ can be labeled as edge and non-edge pixels. More specifically, let C be the set of linear indices corresponding to the edge pixels in the intensity gradient map. Similarly, denote the set of linear indices of non-edge pixels as $C^{\complement}$. Note that these sets account for the indices from all the spectral bands. The sets C and $C^{\complement}$ are now used to determine the MR decimation matrix for a factor $\Delta - 1$, denoted as $\mathbf{D}_{\Delta-1}$ which allows the reconstruction of the data cube $\hat{\mathbf{F}}_{\Delta-1}$. Recall that the main idea is that $\mathbf{D}_{\Delta-1}$ employs a decimation factor $2^{\Delta-1}$ for pixels in C (edges) and 2^{Δ} for pixels in $C^{\complement}$ (non-edges). Therefore, the entries of $\mathbf{D}_{\Delta-1}$ are determined by the entries of two different decimation matrices: $\tilde{\mathbf{D}}_{\Delta}$ and $\tilde{\mathbf{D}}_{\Delta-1}$, each one designed to spatially down-scale all data cube voxels by factors Δ and $\Delta - 1$, respectively. In general, non-zero entries in a row of the decimation matrix indicate the linear indices of the pixels that will be grouped into the super-pixel indexed by that particular row. Let us first consider the case in which the i-th pixel belongs to C, i.e. it is part of an image edge. Accordingly, the i-th row of $\mathbf{D}_{\Delta-1}$ is obtained by selecting the i-th row of $\tilde{\mathbf{D}}_{\Delta-1}$. On the other hand, when i does not index an edge pixel, $i \in C^{\complement}$, the i-th row of $\mathbf{D}_{\Delta-1}$ is a selected row from $\tilde{\mathbf{D}}_{\Delta}$. Mathematically, the $i-$th row of the MR decimation matrix can be written as

$$(\mathbf{D}_{\Delta-1})_i = \begin{cases} (\boldsymbol{\chi}_{\Delta-1})_i \, \tilde{\mathbf{D}}_{\Delta-1} & , i \in C \\ (\boldsymbol{\chi}_{\Delta})_{i'} \, \tilde{\mathbf{D}}_{\Delta} & , i \in C^{\complement} \\ 0 & , \text{otherwise} \end{cases}, \tag{9}$$

where $(\boldsymbol{\chi}_{\Delta-1})_i$ represents the selection of the $i-$th row of a matrix by a circulant permutation matrix. Figure 3 illustrates a toy example of the MR decimation matrix in (9) for $N = 8$, $L = 1$, $\Delta = 2$, which means that a 4×4 data cube would be recovered in this case. The dotted rectangle highlights a row corresponding to a non-edge pixel for which the correspondent row from $\tilde{\mathbf{D}}_2$ indexed by i' is assigned to the $i-$th row of $\mathbf{D}_1$. Similarly, the solid rectangle indicates an edge pixel for which the $i-$th row of $\tilde{\mathbf{D}}_1$ is mapped directly to the $i-$th row of $\mathbf{D}_1$. Note that the index i' represents a row mapping due to the scaling process. The reconstruction of $\hat{\mathbf{F}}_{\Delta-1}$ can thus be

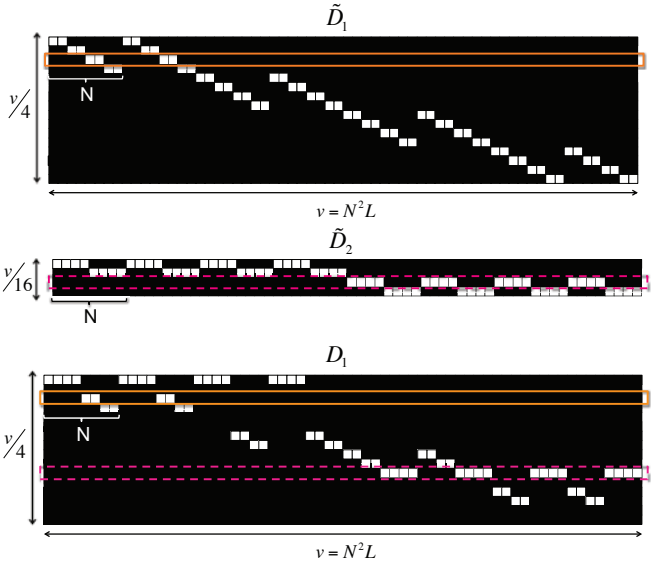

Fig. 3. Example of the MR decimation matrix $\mathbf{D}_1$ generated from the decimation matrices $\tilde{\mathbf{D}}_1$ and $\tilde{\mathbf{D}}_2$. Illustrated matrices correspond to a data cube of spatial resolution $N = 8$, and $L = 1$ spectral band.

obtained solving the problem from (6) using $\tilde{\mathbf{H}} = \mathbf{H}\mathbf{D}^{T}_{\Delta-1}$. Because smooth regions are recovered at a larger decimation factor, which means that pixel indices belonging to $C^{\complement}$ lie on a larger pixel grid, each final spectral band is retrieved by replicating the recovered smooth pixels in a 2×2 window, and keeping the edge recovered pixels. It is worth noting that the

ISBN 978-90-827970-1-5

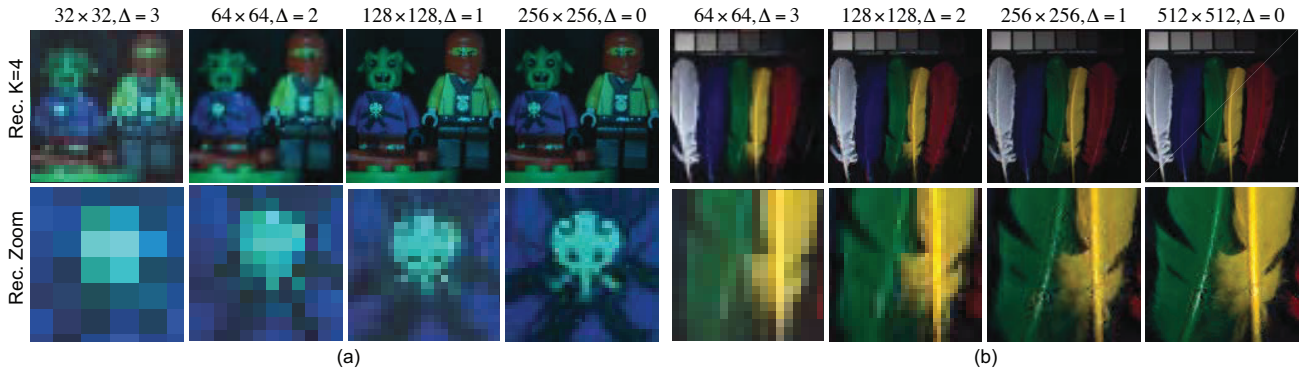

Fig. 4. Noiseless MR reconstructions from $K = 4$ snapshots and different decimation factors (Δ), along with zoomed portions for (a) Toys and (b) Feathers.

whole process can be generalized for several iterations $t = 0, \cdots, \Delta$, such that the decimation factors to recover $\hat{\mathbf{F}}_{\Delta-t}$ can be written as $\Delta - t$ for edge pixels and $\Delta - t + 1$ for non-edge pixels.

IV. Simulations and Results

Simulations were performed to test the proposed MR reconstruction approach, using two different spectral data cubes: Toys and Feathers with 256×256 and 512×512 pixels of spatial resolution, respectively, and $L = 8$ spectral bands [21]. The experiments were performed by simulating the CASSI architecture with blue noise coded (BN) apertures [20], varying the number of snapshots K from 2 to 8. The regularization parameter was found by cross validation. Figure 4 illustrates RGB mappings of the recovered data cubes using the proposed MR reconstruction approach for different decimation factors, i.e. $\Delta = 0, 1, 2, 3$. Zoomed portions of each reconstruction are also included to illustrate the loss of details while the decimation factor increases. Furthermore, for the case of the Toys data cube, $\Delta = 3$ represents an extreme case because a $32 \times 32 \times 8$ data cube is obtained, in which shapes are preserved but details cannot be recovered.

Because interpolations can also be used to upscale low resolution images, Fig. 5 presents a comparison of average reconstruction quality measured as the peak signal-to-noise ratio (PSNR) between the proposed MR reconstruction approach and results from interpolated low resolution data cubes, from noisy measurements with two levels of Gaussian noise SNR$= 10, 20$ dB. Specifically, low resolution versions of the data cubes were individually recovered using (6) with $\tilde{\mathbf{H}} = \mathbf{H}\tilde{\mathbf{D}}_{\Delta}$ for $\Delta = 1, 2, 3$. These small data cubes were afterwards interpolated to a target resolution of 256×256 for Toys and, 512×512 for Feathers, using a bicubic interpolator. These results are compared with the proposed MR reconstruction approach with $\Delta = 3$, such that the initial low resolution approximation exhibits $1/8$ of the maximum attainable resolution. Average PSNR values presented in Fig. 5 are calculated with respect to the correspondent decimated version of the ground truth. In general, these results show that the proposed approach provides better reconstruction quality than interpolation. Also, it can be noted that the interpolation reconstruction quality increases as the ratio between the initial and target resolutions decreases. However, the MR reconstruction approach shows an improvement of up to 3dB of PSNR with respect to the best interpolation case. Figures 6 and 7 illustrate an RGB mapping of the attained 256×256 Toys and 512×512 Feathers reconstructions from $K = 4$ snapshots, respectively. In particular, these figures present the MR reconstructions from $\Delta = 3$, and the bicubic interpolations from the lower resolution versions from Fig. 5. It is easy to see that interpolations are not able to provide accurate reconstructions of the high frequency components of the scenes.

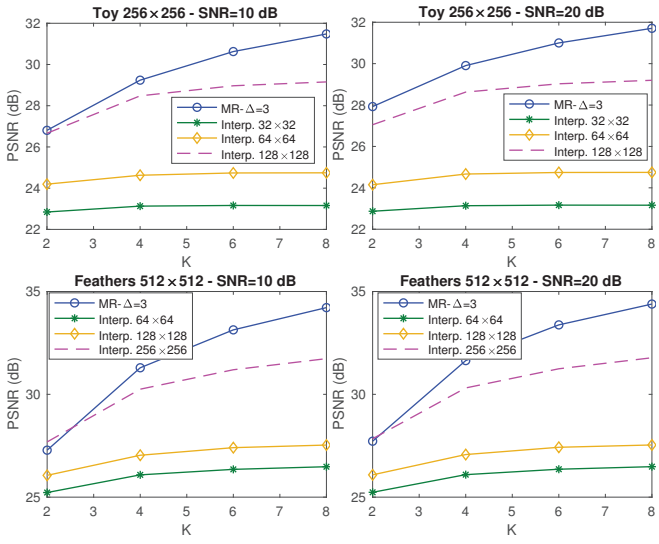

Fig. 5. Average reconstruction PSNR as a function of the number of snapshots K, for 256×256 Toys and 512×512 Feathers using MR with $\Delta = 3$, and bicubic interpolations from lower resolution recovered data cubes and Gaussian noise with SNR=10, 20.

The cost of CSI reconstructions depends on the dimensions of the signal to recover. It has been previously shown that general iterative algorithms that solve (1) perform $O\left(KN^4L\right)$ floating point operations per iteration to recover a $N \times N \times L$ data cube [1]. These operations include matrix products, matrix pseudoinverses, and sparse transformations. Because

ISBN 978-90-827970-1-5

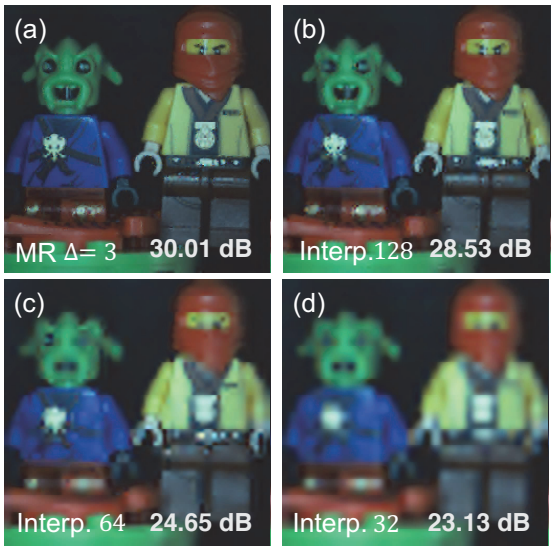

Fig. 6. RGB profiles of 256×256 Toy reconstructions from noisy measurements with SNR=20, for (a) MR-$\Delta = 3$, and interpolations from (b) 128×128, (c) 64×64, and (d) 32×32 reconstructions.

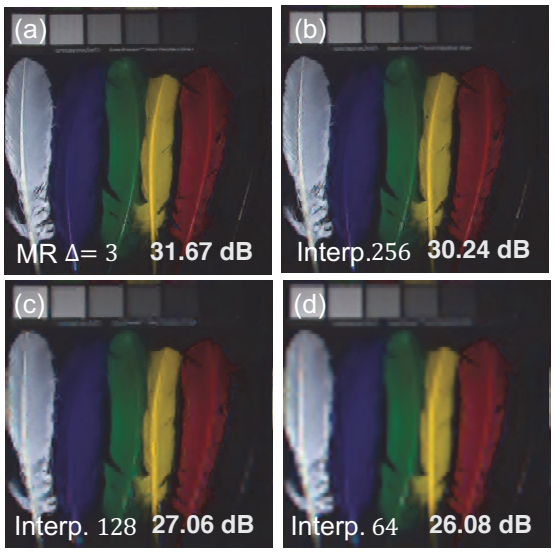

Fig. 7. RGB profiles of 512×512 Feathers reconstructions from noisy measurements with SNR=20 for (a) MR-$\Delta = 3$, and interpolations from (b) 256×256, (c) 128×128, and (d) 64×64 reconstructions.

the proposed approach recovers a $N/2^{\Delta} \times N/2^{\Delta} \times L$ spectral cube, the number of operations per iteration is reduced to $O\left(\frac{KN^4L}{16^{\Delta}}\right)$. The effect on other CS reconstruction formulations is currently under study.

V. Conclusions

A MR reconstruction approach from compressive spectral coded projections has been presented. The proposed approach exploits a map of intensity gradients of a low resolution reconstruction, obtained from the high resolution projections, to generate a MR decimation matrix that groups low frequency areas of the scene into larger super pixels. Thus, multiple versions of the data cube can be sequentially attained, each one employing the previous recovered data cube. Simulations show that the proposed approach improves reconstruction quality in up to 3dB of PSNR with respect to interpolation in noisy scenarios. Furthermore, the amount of floating point operations per reconstruction iteration is reduced by a factor of $1/16^{\Delta}$ with respect to the full resolution reconstruction.

References

[1] G. R. Arce, D. J. Brady, L. Carin, H. Arguello, and D. S. Kittle, "Compressive coded aperture spectral imaging: An introduction," *IEEE Sig. Proc. Mag.*, vol. 31, no. 1, pp. 105–115, 2014.

[2] A. A. Wagadarikar, R. John, R. Willett, and D. Brady, "Single disperser design for coded aperture snapshot spectral imaging," *Appl. Opt.*, vol. 47, pp. B44–B51, 2008.

[3] X. Lin, G. Wetzstein, Y. Liu, and Q. Dai, "Dual-coded hyper-spectral imaging," *Opt. Letters*, vol. 39, no. 7, pp. 2044–2047, 2014.

[4] X. Lin, Y. Liu, J. Wu, and Q. Dai, "Spatial-spectral encoded compressive hyperspectral imaging," *ACM Trans. on Graphics*, vol. 33, no. 6, pp. 233:1–233:11, 2014.

[5] C. V. Correa, H. Arguello, and G. R. Arce, "Snapshot colored compressive spectral imager," *J. Opt. Soc. Am. A*, vol. 32, no. 10, pp. 1754–1763, Oct 2015.

[6] G. R. Arce, H. Rueda, C. V. Correa, A. Ramirez, and H. Arguello, *Snapshot Compressive Multispectral Cameras*. John Wiley & Sons, Inc., 2017.

[7] D. L. Donoho, "Compressed sensing," *IEEE Trans. Information Theory*, vol. 52, no. 4, pp. 1289–1306, 2006.

[8] E. J. Candès and M. B. Wakin, "An introduction to compressive sampling," *IEEE Sig. Proc. Mag.*, vol. 25, no. 2, pp. 21–30, 2008.

[9] T. Gelvez, H. Rueda, and H. Arguello, "Joint sparse and low rank recovery algorithm for compressive hyperspectral imaging," *Appl. Opt.*, vol. 56, no. 24, pp. 6785–6795, 2017.

[10] M. Golbabaee and P. Vandergheynst, "Hyperspectral image compressed sensing via low-rank and joint-sparse matrix recovery," in *2012 IEEE ICASSP*, 2012, pp. 2741–2744.

[11] J. Tian, Y. Ma, H. Rueda, D. Baron, and G. R. Arce, "Compressive hyperspectral imaging via approximate message passing," *IEEE J. of Selected Topics in Signal Processing*, vol. 10, no. 2, pp. 389–401, 2016.

[12] C. A. Metzler, A. Maleki, and R. G. Baraniuk, "From denoising to compressed sensing," *IEEE Trans. on Information Theory*, vol. 62, no. 9, pp. 5117–5144, 2016.

[13] Y. Fang, L. Chen, J. Wu, and B. Huang, "Gpu implementation of orthogonal matching pursuit for compressive sensing," in *2011 IEEE 17th International Conference on Parallel and Distributed Systems*, 2011, pp. 1044–1047.

[14] M. F. Duarte and R. G. Baraniuk, "Kronecker compressive sensing," *IEEE Trans. on Im. Proc.*, vol. 21, no. 2, pp. 404–504, 2012.

[15] Y. Rivenson and A. Stern, "Compressed imaging with a separable sensing operator," *IEEE Sig. Proc. Letters*, vol. 16, no. 6, pp. 449–452, 2009.

[16] S. Yang, M. Wang, P. Li, L. Jin, B. Wu, and L. Jiao, "Compressive hyperspectral imaging via sparse tensor and nonlinear compressed sensing," *IEEE Trans. on Geoscience and Remote Sensing*, vol. 53, no. 11, pp. 5943–5957, 2015.

[17] H. Arguello, C. V. Correa, and G. R. Arce, "Fast lapped block reconstructions in compressive spectral imaging," *Appl. Opt.*, vol. 52, no. 10, pp. D32–D45, 2013.

[18] T. Goldstein, L. Xu, K. F. Kelly, and R. Baraniuk, "The stone transform: Multi-resolution image enhancement and compressive video," *IEEE Trans. on Im. Proc.*, vol. 24, no. 12, pp. 5581–5593, 2015.

[19] X. Wang and J. Liang, "Multi-resolution compressed sensing reconstruction via approximate message passing," *IEEE Trans. on Computational Imaging*, vol. 2, no. 2, pp. 218–234, 2016.

[20] C. V. Correa, H. Arguello, and G. R. Arce, "Spatiotemporal blue noise coded aperture design for multi-shot compressive spectral imaging," *J. Opt. Soc. Am. A*, vol. 33, no. 12, pp. 2312–2322, 2016.

[21] "Multispectral image database," *Available at http://www.cs.columbia.edu/CAVE/databases/multispectral/*.

ISBN 978-90-827970-1-5